Available online at www.sciencedirect.com
SCIENCE DIRECT
Polymer 46 (2005) 5758–5766
polymer
www.elsevier.com/locate/polymer

Preparation and rheology of polyamide-6/attapulgite nanocomposites and studies on their percolated structure

Liang Shen, Yijian Lin, Qiangguo Du*, Wei Zhong, Yuliang Yang

The Key Laboratory of Molecular Engineering of Polymer, Ministry of Education, Department of Macromolecular Science, People's Republic of China and Fudan University, No. 220, Handan Road, YangPu, Shanghai 200433, People's Republic of China

Received 16 January 2005; received in revised form 18 April 2005; accepted 2 May 2005
Available online 4 June 2005

Abstract

The polyamide-6/attapulgite nanocomposites were prepared via an in situ polymerization route with attapulgites pre-modified with cetyltrimethylammonium bromide (CTAB) and toluene-2,4-diisocyanate (TDI). Morphology observation showed that the exfoliated attapulgite fibers were well dispersed in the polyamide-6 matrix on a nanometer scale and formed a percolation network structure. The rheological behaviors of such polymer/fibrous clay nanocompostie samples were investigated by an ARES rheometer with parallel plate geometry. The storage moduli (G'), loss moduli (G''), and dynamic viscosities of these samples increased monotonically with attapulgite content at low frequencies. The presence of attapulgites caused these nanocomposite melts to have solid-like behaviors and slower relaxation. This behavior can be explained in terms of the development of a grafting-percolated fibrous-silicate network structure. Monte Carlo simulations were performed to determine the critical threshold for attapulgites fibers in 3D. The calculated critical threshold from simulations fitted the results of our rheological experiments very well.

Keywords: Polyamide/silicate nanocomposite; Rheology; Percolation

1. Introduction

Polymeric nanocomposites are composed of polymers and dispersed inorganic particles with at least 1D at nanoscale [1]. Previous studies [2–15], among which a significant part was done by Krishnamoorti and Giannelis, addressed the linear and nonlinear viscoelastic properties of intercalated and exfoliated layered-silicate nanocomposites of homopolymers and disordered block copolymers. Those studies found that the quiescent state dispersion of the silicate layers (usually montmorillonite) and its ability to form percolated network structures dominate the linear viscoelastic response. A solid-like behavior, i.e. a finite apparent yield stress is observed for exfoliated montmorillonite with silicate loading as low as 3 wt% while for intercalated montmorillonite with approximately 5 wt%. However, the nonlinear viscoelastic properties of those composites, although affected by the state of dispersion, are mainly controlled by the orientation of the layers under external flow and may vary dramatically according to the strength of the polymer/layered silicate interactions. Recently there were reports of research on polyamide-6 based layered silicate nanocomposites with as little as 1–2 vol% (3–4 wt%) layered silicate [16–19], which provided significant information on the static and dynamic properties of confined polymers. The rheological properties of these materials are closely related to the distortion or deformation of the nanocomposites. And the rheological properties of particulate suspensions are linked to the structure, particle size, shape, and surface characteristics of the dispersed phase. Therefore, understanding rheological properties of polymer melt layered silicate nanocomposites is crucial for gaining the insight of the processability and structure–property relations of these materials. Rheology study also offers a means to assess the state of dispersion of nanocomposites directly in the melt state.

In regard to nanocomposites of the polyamides, a larger number of reports [20–28] have focused on the intercalation and blending methods used to prepare polyamide/clay

* Corresponding author. Tel.: +86 21 6564 3891; fax: +86 21 6564 0293.
E-mail address: qgdu@fudan.edu.cn (Q. Du).

0032-3861/$ - see front matter © 2005 Elsevier Ltd. All rights reserved.
doi:10.1016/j.polymer.2005.05.040

nanocomposites, in which the original work was done by the researchers at Toyota. When preparing for nanocomposites with alumino-silicate layers such as montmorillonites, the inorganic phase cannot be evenly dispersed on a nanometer scale simply by intercalation and blending methods, therefore processes involving swelling and cation exchange are usually needed. In situ polymerization, where inorganic particles are dispersed in an appropriate monomer and followed by heat treatment of the reaction mixture to induce polymerization, has been used to prepare composites. With this method, inorganic particles can be evenly dispersed in the polymer matrix, resulting in composites with improved processability and good thermal and mechanical properties [29–32].

Attapulgite is a family of fibrous hydrous magnesium silicates [33]. The structure of attapulgite was first proposed by Bradley, who described a theoretical half unit-cell formula $Mg_5Si_8O_{20}(OH_2)_2(OH)_4 \cdot 4H_2O$ [34]. The chemical structure of the attapulgite is given in Fig. 1. This structure of fibrous minerals differs from that of other layered silicates used in nanocomposites in which they lack continuous octahedral sheets such as montmorillonite. Attapulgite has a large surface area and strong absorptive capacity that is greater than any other natural mineral [33]. In addition it had good mechanical strength and thermal stability. These properties make attapulgite an ideal material for reinforcement. In the preparation of a polyamide-6/attapulgite nanocomposite, the most important step is the activation of the attapulgite fibers, which is to support active organic groups onto the surface of the fibers [35]. To date, very little is known about polymer/fibrous clay (such as attapulgites) systems from the rheological point of view.

In this article, we present a convenient, in situ polymerization route for the preparation of polyamide-6/attapulgite nanocomposites using cetyltrimethylammonium bromide (CTAB) and toluene-2,4-diisocyanate (TDI) for attapulgites' interfibrillar modification. The rheology of a series of polyamide-6/attapulgite nanocomposites were investigated using a parallel-plate mode. The influence of varying loading of the fibrous silicate on the linear and nonlinear viscoelastic properties was examined. The results were interpreted in terms of solid-like behavior and percolated network structure in light of the recent development of rheological studies of polymer/layered silicate nanocomposites. The similarities and differences of rheological responses of these two kinds of clay-based nanocomposites were also demonstrated. Monte Carlo computer simulations with a 3D stick model were performed on a cubic lattice model to explain the transition of the rheological property, and the critical percolation thresholds for the randomly oriented stick objects were calculated based on the polymer chains considered.

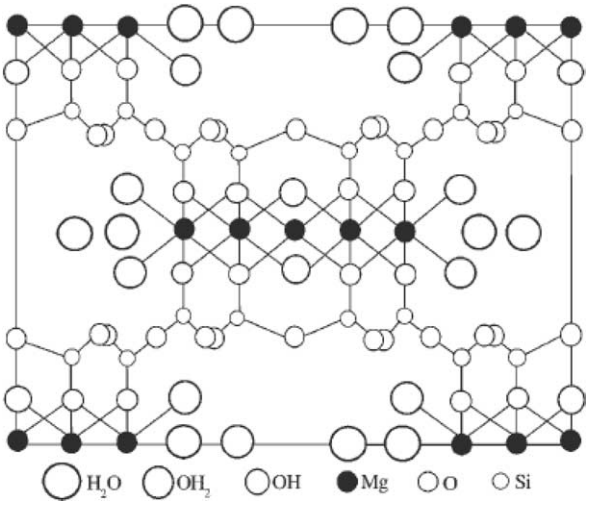

Fig. 1. The chemical structure of attapulgite.

2. Experimental

2.1. Materials

ε-Caprolactam, ε-amino-caproic acid (chemical reagent grade), cetyltrimethylammonium bromide (CTAB), formic acid (98%), and sodium chloride (analytical reagent grade) were purchased from Shanghai Chemical Reagents Company and used without further purification. Attapulgite (CEC = 25–30 mequiv/100 g) was generously provided by Junda Attapulgite Material Co., Ltd (Guiwu Town, Xuyi County, Jiangsu Province, PRC). Toluene-2,4-diisocyanate (TDI) and dibutyltin dilaurate (DBTD) were purchased from Shanghai Lingfeng Chemical Reagent Co., Ltd and used without purification.

2.2. Preparation of CTAB-attapulgite

CTAB-attapulgite was prepared by adding the equivalent amount of CTAB drop-wisely in about 2 h to a 5 wt% Na-attapulgite suspension formulated after being ion-exchanged in NaCl solution. Assisted with ultrasonic agitation the suspension was filtered. The product was washed three times with de-ion water, dried in a vacuum oven and then ground.

2.3. Selective interfibrillar modification of CTAB-attapulgite with TDI

Fifteen grams of CTAB-attapulgite were dispersed in 600 mL of toluene. The dispersion was refluxed for 20 min. After removing the intercalary water, 10.45 g of TDI and three drops of DBTD were added into the CTAB-attapulgite/toluene system. The mixture was left to react at 60 °C for 4 h. The suspension was filtered and the product CTAB-attapulgite-TDI was dried in a vacuum oven. The grafting process was shown in Scheme 1.

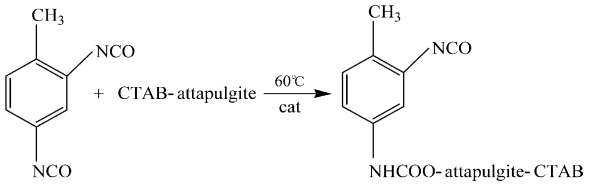

Scheme 1. Grafting reaction of CTAB-attapulgite with TDI.

2.4. Synthesis of polyamide-6/attapulgite nanocomposites

Ninety grams of ε-caprolactam, 10 g of ε-amino-caproic acid and the corresponding amount of attapulgite were mixed in a 250 mL four-necked flask equipped with a mechanical stirrer, a thermometer with a temperature controller, and a nitrogen inlet. The ring-open polymerization of ε-caprolactam was carried out at 250 °C for 5 h under nitrogen. The products were mechanically crushed and soaked in boiling water for 1 h to extract unreacted monomer and oligomers, and then dried at 105 °C under vacuum for 24 h.

2.5. Charaterization

Fourier-transform infrared analyses were recorded on a Nexus-470 FTIR spectrophotometer (Nicolet Instruments, USA). Transmission electron micrographs were obtained using a HITACHI H-600 electron microscope operated at an acceleration voltage of 100 kV. The powder samples of attapulgite were fully dispersed in distilled water. The morphologies of the fracture surfaces of the polyamide-6/attapulgite nanocomposites, which were broken off in liquid nitrogen and coated with Platinum, were observed by a JSM-5600LV scanning electron microscope (JEOL Corporation, Japan). Rheology measurements were undertaken using a parallel-plate mode of Rheometric Scientific ARES (USA), and the test samples were prepared by injection moulding. The diameter of both upper and lower plates was 25 mm, and the gap between the two parallel plates was 1.7 mm. The measurements were conducted with a 200 g cm transducer with a lower resolution limit of 0.2 g cm over a frequency range of 10^{-1}–10^{2} rad s^{-1} at 260 °C.

3. Results and discussion

3.1. The structure and the morphology

In comparison with the spectrum of virgin attapulgites (Fig. 2(a)), the spectrum of CTAB-attapulgite samples (Fig. 2(b)) has the absorption at 2922 and 2845 cm^{-1} which due to the oscillation of C–H bond, reflecting the success of the organic modification of the original attapulgites. The absorption at 2270 cm^{-1} in Fig. 2(c) is characteristic of the –N=C=O group of TDI, indicating that after grafting

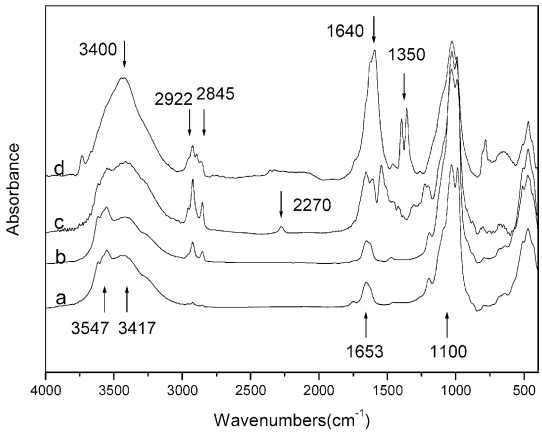

Fig. 2. FTIR spectra of original attapulgite (a), attapulgite-CTAB (b), TDI-attapulgite-CTAB (c) and silicates isolated from polyamide-6/attapulgite nanocomposites (d).

reaction there are remaining *ortho*-N=C=O groups which can be react with the amino groups or the carbonyl groups of ε-caprolactam during its ring-open polymerization. The absorption bands at 1538, 1609, 1653 cm^{-1} are due to the deformation vibration of –NH– and carbonyl, signaling the interfibrillar reaction.

To confirm the grafting reaction between attapulgite and polyamide-6 matrix via TDI molecules, the nanocomposites were thorough washing with formic acid to remove all homopolymers. The remaining modified attapulgites were chatacterized by FTIR as shown in Fig. 2(d). The modified attapulgites have several new peaks in their FTIR spectra when compared with virgin attapulgites. The peaks at 1640 and 1350 cm^{-1} are of polyamides, while the peaks at 2920 and 2845 cm^{-1} represent the oscillation of the C–H bond, and that near 3400 cm^{-1} corresponds to N–H bonds. These results verified that some polyamide-6 molecules had been grafted onto the attapulgite surface through chemical bonding rather than physical absorption.

The absorption band at 3417 cm^{-1} is ascribed to the surface –OH groups of the attapulgite-CTAB. The absorption bands at 3547 and 1640 cm^{-1} are due to the stretching vibration and deformation vibration of the interfibrillar water. The interfibrillar water in the attapulgite-CTAB should be removed since it reacts with TDI and is harmful to the interfibrillar grafting reaction. The FTIR spectra in Fig. 2 show the effectiveness of removing the interfibrillar water by codistillation with toluene. By comparing the spectrum of original attapulgite with those of attapulgite-CTAB and TDI-attapulgite-CTAB in Fig. 2, it can be seen that after codistilled with toluene, the absorption bands at 3547 and 1640 cm^{-1} become much smaller in Fig. 2(c), indicating that most interfibrillar water can be removed by distillation with toluene.

Attapulgite can be characterized by its fibrous morphology. TEM photograph shows attapulgite is a randomly oriented network of densely packed fibers (Fig. 3). The diameter of a single fiber is about 20–40 nm, and the length

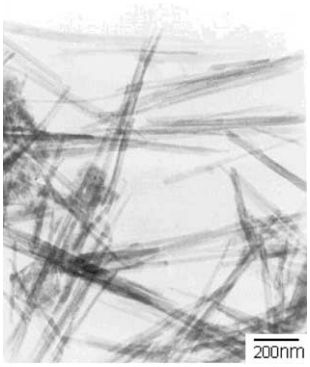

Fig. 3. TEM image of original attapulgite.

of a fiber is between 1 and 2 μm. Thus, the mean value of the aspect ratios of the length to the diameter of a fiber ($L/2R$) is in the range of 30–40.

Fig. 4 are SEM images of typical polyamides-6/attapulgite nanocomposites with surface etched with formic acid. It is clear that the silicate fiber sticks of the clay crystallites were dispersed in the polyamide-6 matrix on a nanometer scale and the increasing clay loading indicates the success of our route for preparation. Also, the edges of the crystallites appeared to be better dispersed into the surrounding matrix.

Furthermore, SEM images demonstrate that the exfoliated attapulgite fibers are anisotropically dispersed in the polymer matrix without being broken. The diameter of a single fiber is still 20–40 nm. On the basis of this mesoscopic structure it is reasonable to assume that at low silicate concentrations (Fig. 4(A)) the relative orientations of the single fibers are uncorrelated while beyond a critical volume fraction (Fig. 4(B)) the occasional individual fibers are incapable of rotating freely and are prevented from relaxing completely when subjected to small-amplitude shear. This incomplete relaxation due to the physical jamming or percolation of the nanoscopic fillers leads to the presence of the solid-like behavior. It is expected that other viscoelastic signatures consistent with that of a percolated system, and these will be discussed in the following rheology studies.

3.2. Rheology of the nanocomposites

The linear dynamic viscoelastic master curves for the series samples of polyamide-6/attapulgite nanocomposites are shown in Fig. 5. The measurement of rheological properties of polymeric materials at molten state is crucial to gain fundamental understanding of the processability and the structure-property relationship for these materials.

Fig. 5(A) shows that the regions of linear viscoelastic behavior for all the samples are very wide and insensitive to the presence of modified attapulgite. The linear viscoelastic regions extend to a strain of 20% under the testing condition. Fig. 5(B)–(D) indicated that the addition of clay has significant effect on the samples' linear dynamic viscoeleastic response especially at the low frequency region. As expected, the moduli and complex viscosities of the nanocomposites increase with increasing silicate loading at all frequencies. At high frequencies, the qualitative behavior of G' and G'' is essentially the same. However, at low frequencies, polyamide-6/attapulgite nanocomposites melts have higher storage moduli (G'), loss moduli (G''), and complex viscositis when compared with neat polyamide-6 and show a montonic increase with attapulgite content.

At the temperatures and frequencies used for the rheological measurements the polyamide-6 polymer chains are fully relaxed and exhibit characteristic homopolymer-like terminal behavior, i.e. $G' \propto \omega^2$ and $G'' \propto \omega$, which is similar to the behavior of melts of homopolymer of narrow M_w distribution. On the other hand, the viscoelastic response (particularly, G') for all nanocomposites display significantly diminished frequency dependence as compared to the matrices. In fact, for all the Polyamide-6/attapulgite samples, G' and G'' becomes nearly independent of frequency at low frequency range, which is characteristic of materials exhibiting solid-like behavior, i.e. $G' \propto \omega^0$ and $G'' \propto \omega^0$.

The frequency dependence of the storage modulus at low-frequency-regime decreases monotonically with the increase of silicate loading, from $\omega^{1.98}$ for polyamide-6 to $\omega^{0.56}$ for polyamide-6/5 wt% attapulgite at 260 °C. The frequency dependence of G'' also progressed monotonically with silicate loading, from $\omega^{1.11}$ for polyamide-6 to nearly

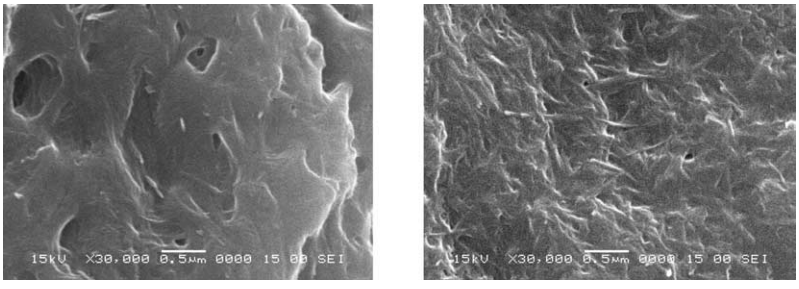

Fig. 4. The SEM image of the typical sample of polyamide-6/attapulgite nanocomposites with surface etched with formic acid. A: With 2 wt% attapulgite content; B: with 5 wt% attapulgite content.

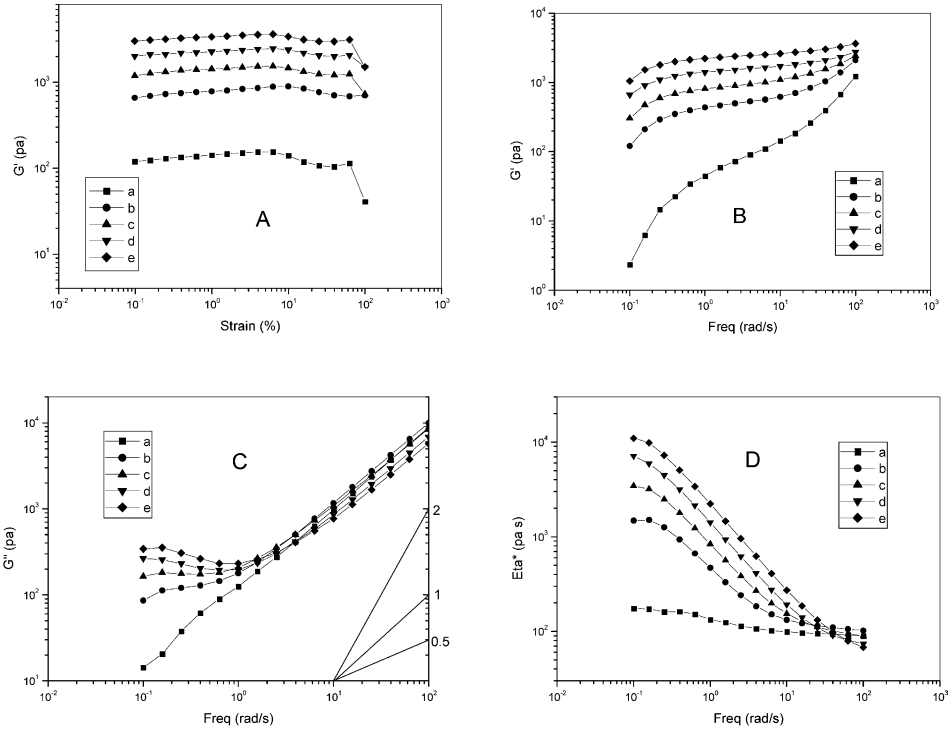

Fig. 5. Small amplitude frequency sweep data at 260 °C for series of polyamide-6/attapulgite nanocomposites: (a) neat polyamide-6 and polyamide-6 with attapulgite loading at (b) 2 wt%, (c) 3 wt%, (d) 4 wt%, (e) 5 wt%. (A) Comparison of dynamic stain sweep data; (B) storage moduli as a function of frequency; (C) loss moduli as a function of frequency; (D) complex viscosity as a function of frequency.

ω^0 for Polyamide-6/5 wt% attapulgite at 260 °C. The frequency dependence data of G' and G'' for all the samples is summarized in Table 1.

The frequency dependence of G' and G'', at low frequency region wherein a solid-like behavior is observed for the nanocomposites, is similar to that observed previously from end-tethered poly(ε-caprolactone)-based exfoliated nanocomposites [3]. It was then proposed that, due to the highly anisotropic nature of the fibrous silicates and simple geometric constraints, the fibers exhibited local correlations [4], which is line with our observation. The lower slope values and the higher absolute values of the dynamic moduli imply the formation of a percolated structure of the dispersed silicate fibers in the polyamide-6 matrix (also observed from the SEM observations). According to this structure, the individual silicate fiber is incapable of free rotation, and hence the relaxation of the structure by imposing small ω is almost completely prevented. This type of hindered relaxation due to the geometric constraints of the stacked silicate fibers leads to the occurance of the solid-like behavior observed in polyamide-6/attapulgite nanocomposites. The incorporation of the nanoscopic, fibrous silicates also causes the increase of the zero shear viscosity in a few orders of magnitude as shown in Fig. 6. In summary, owing to the formation of percolation network structure of attapulgite fibers, the incorporation of the attapulgite silicate fibers in polyamide-6 matrix leads to a solid-like behavior of the nanocomposites. And the moduli and viscositis of the nanocoposites increase with the attapulgite content.

Larson [36] illustrated G' and G'' values for prototypical solid-like and liquid-like materials. Liquid-like behavior is expected when $G' < G''$ and solid-like behavior is predicated when $G' > G''$ and G' is nearly independent of the

Table 1
Slopes of lines of $\log G'$ and $\log G''$ vs ω at low-frequency region for polyamide-6/attapulgite nanocomposites

Sample	G'	G''
Neat polyamide-6	1.9_8	1.1_1
Polyamide-6/2 wt% attapulgite	1.2_3	0.6_1
Polyamide-6/3 wt% attapulgite	1.0_8	0.2_1
Polyamide-6/4 wt% attapulgite	0.6_8	-0.0_8
Polyamide-6/5 wt% attapulgite	0.5_6	-0.1_4

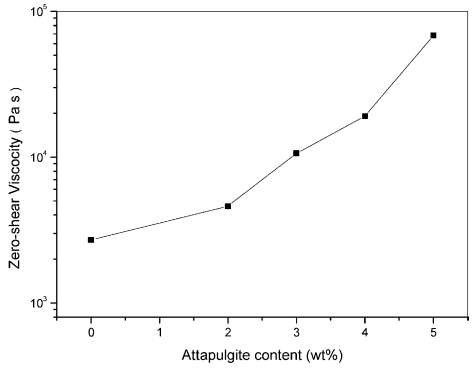

Fig. 6. Plot of zero-shear viscocity vs attapulgite content at 260 °C.

frequency. The frequency response of the G' and G'' of our nanocomposites is shown in Fig. 7. The melt behavior of our samples is liquid-like ($G' < G''$) at high frequencies while solid-like at low frequencies ($G' > G''$), which is opposite to that reported by the previous studies [37,38] on polymer/layered clay nanocomposites. The presence of $G' > G''$ is an indication of the formation of percolation network or physical jamming. And broader frequency ranges for solid-like behavior ($G' > G''$) were observed as increasing attapulgite loading. For neat polyamide-6, it only exhibited liquid-like behavior and no transition from liquid-like to solid-like was found at full frequency range. By inspecting the data of the nanocomposites, it can be seen that the transition from liquid-like behavior to solid-like behavior occurs at the intersection of line G' and line G''. The frequencies at the intersections for all the samples are listed in Table 2. The frequency at the cross point for polyamide/attapulgite nanocomposites shifts towards a higher value with the increase of the clay loading. The liquid-like behavior of these nanocomposites may be related to the orientation of the silicate fibers at high frequency.

The stress relaxation spectrum $H(\tau)$ is related to the dynamic oscillatory shear G' as [39] where the ω is the shear rate and τ is the relax time,

$$H_3'(\tau) = \left[\frac{d^2}{d(\ln \omega)^2} - \frac{1}{4}\frac{d^3}{d(\ln \omega)^3}\right] G'(\omega)|_{1/\omega=\tau}$$

and the results of these are shown in Fig. 8. This approximate relation has proven useful to relate the dynamic and transient moduli for homopolymers. Recently, the same relationship was successfully used to describe the viscoelastic properties of systems with micelles dispersed in a homopolymers [40,41].

From the curves of the relaxation spectrum in Fig. 8, it can be concluded that the dynamic viscoelastic response is a combined of the relaxation of macromolecules motion and the entanglements of polymer melts. For polyamide-6/attapulgite nanocomposite samples, at attapulgite content > 2 wt%, besides the relaxation response of polyamide-6 macromolecules there is another relaxation response

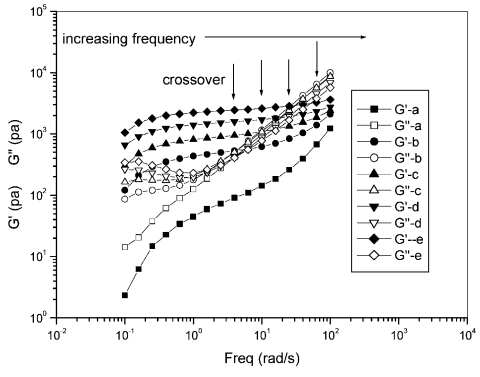

Fig. 7. Plot of G' and G'' vs frequency for the series samples of polyamide-6/attapulgite nanocomposites: (a) neat polyamide-6 and polyamide-6 with attapulgite loading at (b) 2 wt%, (c) 3 wt%, (d) 4 wt%, (e) 5 wt%.

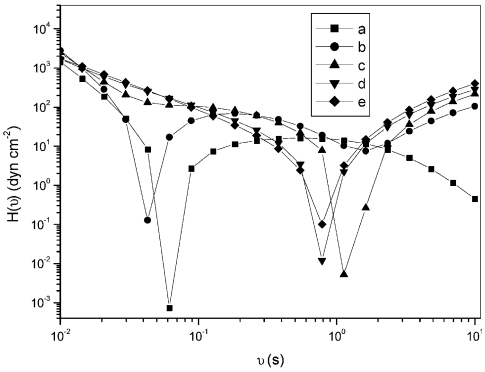

Fig. 8. Relaxation spectrum from master curves of the series samples of polyamide-6/attapulgite nanocomposites at 260 °C: (a) neat polyamide-6 and polyamide-6 with attapulgite loading at (b) 2 wt%, (c) 3 wt%, (d) 4 wt%, (e) 5 wt%.

resulting from an additional network, which is clearly reflected in the region of τ around 1 s. This relaxation corresponding to the physical jamming or percolation of the nanoscpic fillers leads to the presence of the solid-like behavior.

On the basis of both the dynamic oscillatory shear and the stress relaxation moduli, it is clear that the addition of fibrous silicate has a profound influence on the long time relaxation of the nanocomposites and causes them to exhibit 'strongly associated particles' effect. With increasing silicate loading, the liquid-like relaxation observed for the unfilled polymer gradually changes to the solid-like behavior.

3.3. Studies on the percolated structure of the nanocomposites

Based on the findings of our study on the morphology and rheology of polyaimde-6/attapulgite nanocomposites, we propose a 'grafting-percolated' model as shown in Fig. 9(A) to describe its percolated structure. The highly anisotropic attapulgite fibers interconnect with each other and extend on 3D to form a percolated network structure. Each single fiber is confined in a microdomain and prohibited from moving readily due to lack of free space limited by adjacent fibers. The nanocomposites with such silicate framework exhibit solid-like behaviors unless they can overcome the increased activation energy of motion barriers. As the remaining *ortho*-N=C=O groups on TDI-modified attapulgite can react with the amino groups or carbonyl groups on ε-caprolactam during ring-open polymerization, the polymer chains and the silicate fibers are 'bridged' by the grafting junctions provided by TDI. Since the crossing polymer chains have topological constraints and can become entangled, this model also takes account of entanglement constrains for the interpretation of the dynamics of these confined polymer melts.

Krishnamoorti presented a model of a hypothetical hydrodynamic sphere (Fig. 9(C)) and the percolation of

Table 2
The frequency of the transition from liquid-like to solid-like

Sample	Transition frequency
Neat polyamide-6	–
Polyamide-6/2 wt% attapulgite	4
Polyamide-6/3 wt% attapulgite	10
Polyamide-6/4 wt% attapulgite	21
Polyamide-6/5 wt% attapulgite	50

these hydrodynamic spheres to signify the onset of incomplete relaxation and the presence of solid-like behavior in their nanocomposites [4]. From the geometrical point of view, a stick-like model would be a better representation of the silicate fibers in comparison with the sphere model as shown in Fig. 9(B). Therefore in our work Monte Carlo simulations on randomly oriented stick objects were performed to determine the critical percolation threshold.

Previous simulation model and methods [42–47] used permeable stick objects in the form of capped cylinders (cylinders of length L and radius R capped with hemispheres of radius R). For these systems the orientation of fiber was not totally random and a semi-penetrable continuum models was taken. However, our polyamide-6/attapulgite system is a nanocomposites containing long-fiber in which the orientation of the silicate fibers is totally random and the fibers in reality are impenetrable to each other. From this point of view, we consult the lattice model and methods in Isichenko's review [48] and simplify this problem to predict the percolation thresholds of the attapulgite sticks (aspect ratios $L/2R = 30$–40) in our nanocomposites based on the polymer chains considered.

Table 3
Percolation thresholds for our system with different aspect ratios $L/2R$

$L/2R$[a]	Φ_c[b]	W_c[c]
30	0.02197	0.04336
40	0.01756	0.03481

[a] $L/2R$ represents the aspect ratio of the attapulgite stick length to diameter.
[b] Φ_c is calculated in a $300\times300\times300$ lattice model and the results showed in the table are the average values calculated 1000 times.
[c] W_c represents the critical weight fraction of percolation threshold. For the density of the polyamide-6 and the attapulogite silicates is 1.12 and 2.26 g cm^{-3} respectively, we assumed that no other objects occupied the lattice in our defined cube besides the polymer chains and attapulgite fibers.

In our 'grafting-percolated' model, we assume that the 'attapulgite-polymer chain-attapulgite' grafting structure belongs to the percolated structures. Since the root mean square radii of gyration of the polymer chains are about several nanometers, we define one polymer chain occupy one cube ($1\times1\times1$), thus one attapulgite stick should occupy 30 ($30\times1\times1$) or 40 ($40\times1\times1$) cubes. Two attapulgite sticks joined via a polymer chain can be considered as one united entity although they are not

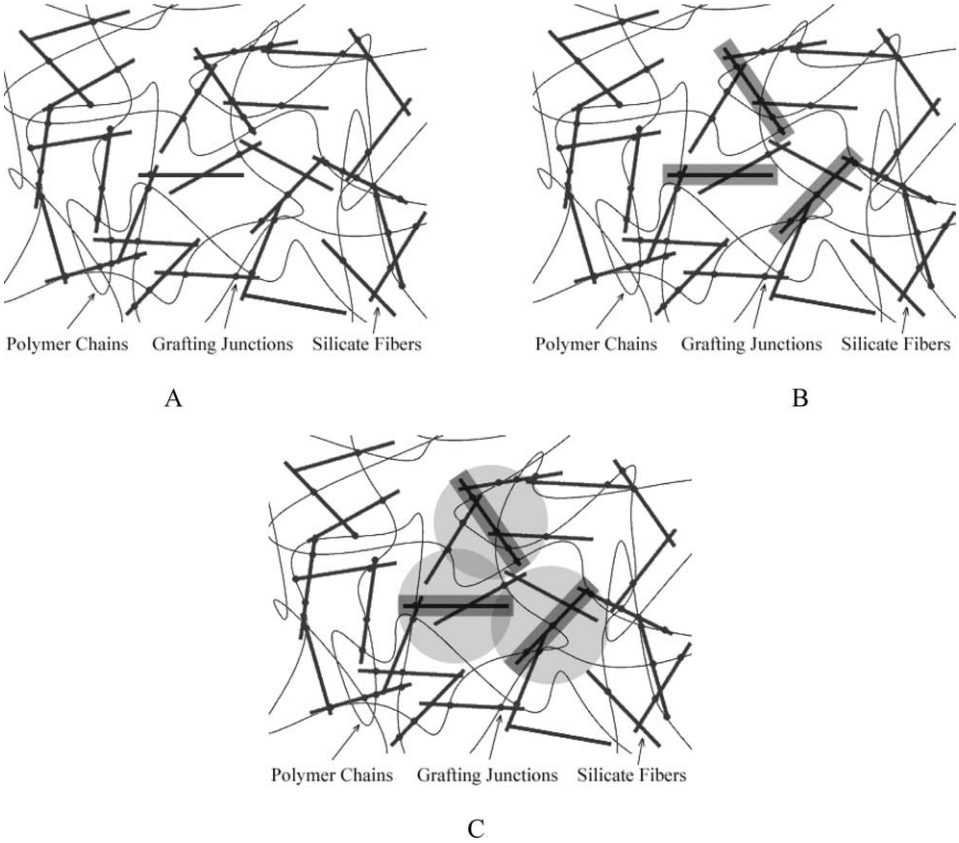

Fig. 9. Schematic diagram describing our polymer/fibrous clay nanocomposites.

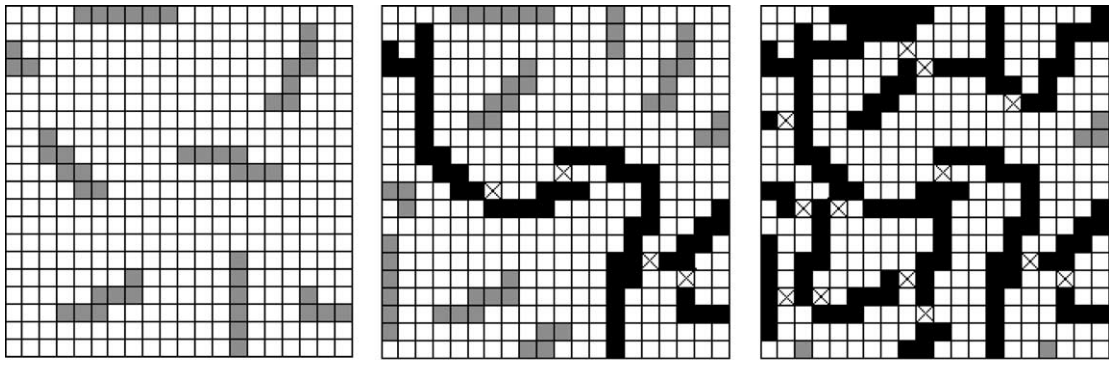

Fig. 10. 2D sketch map of our stick percolation clusters on the square lattice model at $\Phi < \Phi_c$ (A); $\Phi = \Phi_c$ (B); $\Phi > \Phi_c$ (C) with the aspect ratio $L/2R = 6$, in which the black occupied lattices represent the sticks percolated, the grey occupied lattices represent the sticks unpercolated, and the symbols '×' indicate the lattices occupied by the grafted polymer chains.

directly interconnected. Thus, in this percolation lattice model, if the minimum distance between two sticks is within the size of one cube, the two sticks should belong to the same cluster (Fig. 10). Percolation take place when a cluster that can connect the two boundaries ($z = 1$ and $z = 300$) of the 3D-lattice, appears.

The percolation threshold can be expressed as the critical volume (area) fraction Φ_c. The critical volume (area) fraction Φ_c for the randomly oriented sticks with different aspect ratios $L/2R$ were calculated and listed in Table 3. As expected, the percolation threshold is independent of the system size used and decreases with the increase of aspect ratio. Our Φ_c value is much lower by contrast with that reported in Isichenko's review, in which Monte Carlo simulations were used to calculate Φ_c for spheres, discs and other cubic objects [48].

Our Monte Carlo simulation of percolation threshold predicts that percolation will occur at a volume fraction of attapulgite sticks of about 0.02. By measuring density the volume fraction can be converted into weight fraction. In other words, these calculations suggest that percolation emerge at about 3–4 wt% of the fibrous silicate (listed in Table 3). The simulation prediction fits very well with the experimental findings of the rheological studies. Therefore, the Monte Carlo simulation is indeed a useful method for describing such polymer/fibrous silicate nanocomposite system.

4. Conclusions

Polyamide-6/attapulgite nanocomposites were successfully synthesized via in situ polymerization, prior to which attapulgites were modified with cetyltrimethylammonium bromide (CTAB) and toluene-2,4-diisocyanate (TDI). Such grafting-percolated fibrous silicate nanocomposites have many intriguing rheological properties closely related to their composition and structure. The storage moduli, loss moduli, and dynamic viscosities of our nanocomposites show a monotomic increase with attapulgite content in low frequency region due to the confinement of polymer chains and the percolated network structure. The power-law relation in the low frequency region shows a dependence on the concentration of the fibrous silicates and the dependence levels off at about ~5 wt% of silicates. The addition of fibrous silicate has a profound influence on the long time relaxation of the nanocomposites and exhibits 'strongly associated particles' effect. Finally, we provided a 'grafting-percolated' model based on the grafting-percolated structure to explain the solid-like behaviors of such nanocomposites. We also used Mote Carlo simulation to predict critical percolation thresholds of such polymer/fibrous silicates nanocomposites. The predictions of percolation thresholds from the simulation model were in good agreement with experimental results.

Acknowledgements

This work were subsidized by the Special Funds for Major State Basic Research Projects (G1999064800).

References

[1] Giannelis EP, Krishnamoorti RK, Manias E. Adv Polym Sci 1999; 138:107.
[2] Krishnamoorti R, Silva AS. In: Pinnavaia TJ, Beall GW, editors. Polymer-clay nanocomposites. New York: Wiley; 2000.
[3] Krishnamoorti R, Giannelis EP. Macromolecules 1997;30:4097.
[4] Ren JX, Silva AS, Krishnamoorti R. Macromolecules 2000;33:3739.
[5] Krishnamoorti R, Giannelis EP. Langmuir 2001;17:1448.
[6] Krishnamoorti R, Vaia RA, Giannelis EP. Chem Mater 1996;8:1728.
[7] Giannelis EP, Krishnamoorti R, Manias E. Adv Polym Sci 1999;138: 107.
[8] Krishnamoorti R, Ren J, Silva AS. J Chem Phys 2001;108:7175.
[9] Giannelis EP. Adv Mater 1996;8:29.
[10] Galgali G, Ramesh C, Lele A. Macromolecules 2001;34:852.
[11] Hoffmann B, Dietrich C, Thomann R, Friedrich C, Mulhaupt R. Macromol Rapid Commun 2000;21:57.

[12] Solomon MJ, Almusallam AS, Seefeldt KF, Somwangthanaroj A, Varadan P. Macromolecules 2001;34:1864.
[13] Zhong Y, Zhu ZY, Wang SQ. Polymer 2005;46:3006.
[14] Dean D, Walker R, Theodore M, Hampton E, Nyairo E. Polymer 2005;46:3014.
[15] Incarnato L, Scarfato P, Scatteia L, Acierno D. Polymer 2004;45: 3487.
[16] Usuki A, Koiwai A, Kojima Y, Kawasumi M, Okada A, Kurauchi T, et al. J Appl Polym Sci 1995;55:119.
[17] Yano K, Usuki A, Kamigato O. J Polym Sci, Polym Chem 1993;31: 2493.
[18] Usuki A, Kojima Y, Kawasumi M, Okada A, Fukushima Y, Kurauchi T, et al. J Mater Res 1993;8:1174.
[19] Messersmith PB, Giannelis EP. Chem Mater 1993;5:1064.
[20] Kojima Y, Usuki A, Kawasumi M. J Polym Sci, Polym Chem 1993; 31:983.
[21] Kojima Y, Usuki A, Kawasumi M, Okada A, Kurauchi T, Kamigato O. J Appl Polym Sci 1993;49:1259.
[22] Kojima Y, Usuki A, Kawasumi M, Okada A, Kurauchi T, Kamigato O, et al. J Polym Sci, Polym Phys 1994;32:625.
[23] Kojima Y, Matsuoka T, Takahashi H, Kurauchi T. J Appl Polym Sci 1994;51:683.
[24] Kojima Y, Usuki A, Kawasumi M, Okada A, Kurauchi T, Kamigato O, et al. J Polym Sci, Polym Phys 1995;33:1039.
[25] Liu TX, Liu ZH, Ma KX, Shen L, Zeng KY, He CB. Compos Sci Tech 2003;63:331.
[26] Wu TM, Liao CS. Macromol Chem Phys 2000;201:2820.
[27] Fornes TD, Yoon PJ, Hunter DL, Keskkula H, Paul DR. Polymer 2002;43:5915.
[28] Ma CCM, Kuo CT, Kuan HC, Chiang CL. J Appl Polym Sci 2003;88: 1686.
[29] van Zyl WE, Garcia M, Schrauwen BAG, Kooi BJ, Hosson JTMD, Verweij H. Macromol Mater Eng 2002;287:106.
[30] Reynaud E, Jouen T, Gauthier C, Vigier G, Varlet J. Polymer 2001;42: 8759.
[31] Yang F, Ou YC, Yu ZZ. J Appl Polym Sci 1998;69:355.
[32] Ou YC, Yang F, Yu ZZ. J Polym Sci, Polym Phys 1998;36:789.
[33] Leifu R. Clay and clay minerals. China Geology: Beijing; 1992.
[34] Bradley WF. Am Mineral 1940;25:405.
[35] Rong JF, Li HQ, Jing ZH, Hong XY, Sheng M. J Appl Polym Sci 2001;82:1829.
[36] Larson RG. The structure and rheology of complex fluids. New York: Oxford University Press; 1999.
[37] Sung TK, Chung HL, Hyoung JC, Myung SJ. J Polym Sci, Polym Phys 2003;41:2052.
[38] Tae HK, Sung TL, Chung HL, Hyoung JC, Myung SJ. J Appl Polym Sci 2003;87:2106.
[39] Kaschta J, Schwarzl FR. Rheologica Acta 1994;33:517.
[40] Watanabe H, Yao ML, Sato T, Osaki K. Macromolecules 1997;30: 5905.
[41] Sato T, Watanabe H, Osaki K, Yao ML. Macromolecules 1996;29: 3881.
[42] Ogale AA, Wang SF. Compos Sci Technol 1993;46:379.
[43] Wang SF, Ogale AA. Compos Sci Technol 1993;46:389.
[44] Balberg I. Philos Mag B 1987;56:991.
[45] Balberg I, Binenbaum N, Wagner N. Phys Rev Lett 1984;52:1465.
[46] Neda Z, Florian R. Phys Rev E 1999;59:3717.
[47] Ghiass M, Rey AD, Dabir B. Polymer 2002;43:989.
[48] Isichenko MB. Rev Mod Phys 1992;64:961.